Journal of Physics: Conference Series

**PAPER** • **OPEN ACCESS**

# A compressive sensing-based computational method for the inversion of wide-band ground penetrating radar data

To cite this article: A Gelmini *et al* 2017 *J. Phys.: Conf. Ser.* **904** 012002

IOP Conf. Series: Journal of Physics: Conf. Series **904** (2017) 012002 doi:10.1088/1742-6596/904/1/012002

# A compressive sensing-based computational method for the inversion of wide-band ground penetrating radar data

**A Gelmini[1], G Gottardi[1] and T Moriyama[2]**

[1] ELEDIA Research Center (ELEDIA@UniTN - University of Trento)
Via Sommarive 9, I-38123 Trento, Italy
[2] ELEDIA Research Center (ELEDIA@UniNAGA - University of Nagasaki)
852-8521, Nagasaki, Japan
E-mail: {angelo.gelmini, giorgio.gottardi, toshifumi.moriyama}@eledia.org

**Abstract.** This work presents an innovative computational approach for the inversion of wide-band ground penetrating radar (*GPR*) data. The retrieval of the dielectric characteristics of sparse scatterers buried in a lossy soil is performed by combining a multi-task Bayesian compressive sensing (*MT-BCS*) solver and a frequency hopping (*FH*) strategy. The developed methodology is able to benefit from the regularization capabilities of the *MT-BCS* as well as to exploit the multi-chromatic informative content of *GPR* measurements. A set of numerical results is reported in order to assess the effectiveness of the proposed *GPR* inverse scattering technique, as well as to compare it to a simpler single-task implementation.

## 1. Introduction

During the last decades, ground penetrating radar (*GPR*) gained particular attention as a valid prospecting technology in many applicative scenarios dealing with the non-invasive investigation of buried domains, such as, for example, civil engineering, military operations, cultural heritage monitoring, and archaeology [1]-[4]. Thanks to such a success, several inverse scattering methodologies, both deterministic [5]-[8] and stochastic [9],[10], have been proposed to retrieve accurate and easy-to-interpret images of what lies below the interface from *GPR* measurements.

Differently from other prospecting tools, a key feature that characterizes *GPR* is the availability of wide-band data. As a matter of fact, such a frequency diversity can be seen as a powerful source of additional information in order to effectively tackle the *ill-posedness* and *non-linearity* issues of the subsurface imaging problem.

Within this framework, different techniques have been proposed in order to process multi-chromatic data. These approaches can be mainly classified in (*i*) multi-frequency (*MF*) [5],[7],[10] and (*ii*) frequency hopping (*FH*) [6] strategies. On the one hand, *MF* techniques are based on the simultaneous processing of the collected wide-band information [10], while on the other hand *FH* ones process each frequency sample in a cascaded manner, starting from the lowest frequency up to the highest one, and exploiting the acquired information at each step in order to initialize the successive one [6]. Given that, even if *MF* strategies could in principle benefit from a larger amount of information to perform the inversion, they must typically solve a more complex problem with a significantly larger number of unknowns with respect to *FH*-based methodologies.

Moreover, it is worth remarking that in many practical scenarios the unknown buried objects are sparse [5]. Given that, compressive sensing (*CS*)-based techniques [11]-[13] could be seen as an interesting candidate in order to exploit such an *a-priori* information about the nature of the sought solution, by further regularizing the *GPR* inverse scattering problem. Following this line of reasoning, this work presents an innovative inversion methodology that effectively integrates a multi-task Bayesian *CS* (*MT-BCS*) solver [11] within a *FH* strategy in order to retrieve accurate reconstructions of the buried scenario. The *MT-BCS* solution at each stage of the frequency hopping loop is initialized in an innovative way, by exploiting the *acquired* information about the detected scatterers at the lowest frequencies. A set of numerical experiments is presented and discussed, in order to assess the effectiveness of the developed *FH-MT-BCS* technique, and to verify its superiority with respect to a single-task *BCS* (*ST-BCS*)-based implementation.

## 2. *GPR-IS* problem formulation and *FH-MT-BCS* solution approach

Let us consider a two-dimensional scenario consisting of two homogeneous half-spaces separated by a planar interface at $y = 0$. The upper half-space is free-space, while the lower half-space is occupied by a lossy medium having complex permittivity $\varepsilon_{b,eq}(f) = \varepsilon_{rb}\varepsilon_0 - \mathrm{j}\sigma_b/(2\pi f)$. A buried investigation domain $D_{inv}$ is illuminated by a set of $V$ $z$-oriented ideal line sources placed at fixed height above the interface and excited by a wideband current signal. Under the hypothesis that one or multiple targets are present in $D_{inv}$, the electromagnetic interaction between the field radiated by the sources and the half-space scenario generates a measured time-domain total field equal to

$$e_v^{tot}(\mathbf{r}_m, t) = e_v^{scat}(\mathbf{r}_m, t) + e_v^{inc}(\mathbf{r}_m, t); \quad v = 1,...,V\ ; \quad m = 1,...,M \tag{1}$$

where $\mathbf{r}_m$ is the location of the $m$-th receiver above the interface ( $m = 1,...,M$ , $M$ being the number of probes), while $e_v^{inc}(\mathbf{r}_m, t)$ and $e_v^{scat}(\mathbf{r}_m, t)$ denote the incident and scattered fields, respectively. Once $e_v^{scat}(\mathbf{r}_m, t)$ has been isolated from $e_v^{tot}(\mathbf{r}_m, t)$ [8], it is Fourier-transformed to the frequency domain, and a set of $L$ uniformly spaced samples are extracted from the computed *GPR* spectrum within the 3dB bandwidth of the excitation signal ( $f_l \in [f_{\min}, f_{\max}]$, $l = 1,...,L$ ). Accordingly, assuming a contrast source formulation, the following integral equation holds true at each $l$-th frequency

$$E_v^{scat}(\mathbf{r}_m, f_l) = \int_{D_{inv}} G^{ext}(\mathbf{r}_m, \mathbf{r}', f_l) J_v(\mathbf{r}', f_l) d\mathbf{r}'; \quad v = 1,...,V\ ; \quad m = 1,...,M\ ; \quad l = 1,...,L \tag{2}$$

where $G^{ext}(\mathbf{r}_m, \mathbf{r}', f_l)$ is the external Green's function for the buried scenario [10], while $J_v(\mathbf{r}, f_l) = E_v^{tot}(\mathbf{r}, f_l)\tau(\mathbf{r}, f_l)$ is the unknown equivalent current modelling the presence of the unknown objects in $D_{inv}$, $\tau(\mathbf{r}, f_l)$ being the contrast function defined at frequency $f_l$ as follows

$$\tau(\mathbf{r}, f_l) = (\varepsilon_r(\mathbf{r}) - \varepsilon_{rb}) - \mathrm{j}\frac{(\sigma(\mathbf{r}) - \sigma_b)}{2\pi f_l}\ ; \quad l = 1,...,L\,. \tag{3}$$

Assuming an additional noise component on the scattered field and partitioning $D_{inv}$ into $N$ sub-domains, (2) can be arranged in matrix form as follows

$$\tilde{\mathbf{E}}_{v,l}^{scat} = \mathbf{G}_l^{ext}\mathbf{J}_{v,l} + \mathbf{n}_{v,l}\ ; \quad v = 1,...,V\ ; \quad l = 1,...,L \tag{4}$$

where $\mathbf{G}_l^{ext}$ is the $M \times N$ Green's matrix, $\tilde{\mathbf{E}}_{v,l}^{scat} = \left\{\Re\left[\tilde{E}_v^{scat}(\mathbf{r}_m, f_l)\right], \Im\left[\tilde{E}_v^{scat}(\mathbf{r}_m, f_l)\right]; m = 1,...,M\right\}$, $\mathbf{J}_{v,l} = \left\{\Re\left[J_v(\mathbf{r}_n, f_l)\right], \Im\left[J_v(\mathbf{r}_n, f_l)\right]; n = 1,...,N\right\}^T$, while the noise vector is $\mathbf{n}_{v,l} = \left\{\Re\left[n_v(\mathbf{r}_m, f_l)\right], \Im\left[n_v(\mathbf{r}_m, f_l)\right]; m = 1,...,M\right\}$. Accordingly, the solution of the inverse problem at the $l$-th frequency step is formulated within the Bayesian framework as follows

$$\hat{\mathbf{J}}_{v,l} = \arg\left\{\max_{\mathbf{J}_{v,l}} P\left(\mathbf{J}_{v,l} \middle| \tilde{\mathbf{E}}_{v,l}^{scat}\right)\right\}\ ; \quad v = 1,...,V \tag{5}$$

where $P\left(\mathbf{J}_{v,l}\middle|\tilde{\mathbf{E}}_{v,l}^{scat}\right)$ is the posterior probability and $\mathbf{J}_{v,l}$ are correlated among the different views ($v=1,...,V$). The solution of (5) is then found by means of a customized *MT-BCS* solver as

$$\left[\hat{\mathbf{J}}_{v,l}\right]^{opt}=\left[diag\left(\hat{\mathbf{a}}_l\right)+\left(\mathbf{G}_l^{ext}\right)^*\mathbf{G}_l^{ext}\right]^{-1}\left(\mathbf{G}_l^{ext}\right)^*\tilde{\mathbf{E}}_{v,l}^{scat}\ ;\ \ v=1,...,V \tag{6}$$

where $(\cdot)^*$ is the transpose conjugate operator and $\hat{\mathbf{a}}_l=\left\{\hat{a}_{l,n}, n=1,...,N\right\}$ is the shared vector of hyper-parameters estimated through a Relevant Vector Machine (*RVM*) solver.
The estimated contrast function $\hat{\tau}(\mathbf{r}_n, f_l)$, $n=1,...,N$, is then obtained from (6) by averaging over the different views ($v=1,...,V$) the ratio between retrieved currents and the corresponding retrieved total fields.
Since standard *BCS* implementations do not allow to exploit progressively *acquired* information about the solution (i.e., to use the reconstruction at the *l*-th frequency to initialize/guide the $(l+1)$-th step), an innovative "constrained" *RVM* solver has been developed as described in the following. A "filtering and clustering" procedure [6] is applied to the retrieved contrast in order to determine the region of interest (*RoI*) $D_l \subset D_{inv}$ ($D_1=D_{inv}$) in which the buried scatterers have been detected at frequency $f_l$. Then, the solution at frequency $f_{l+1}$ is obtained though a "constrained" *RVM* by solving (6) limiting the search space only to those entries $\hat{a}_{l+1,n}$ of $\hat{\mathbf{a}}_{l+1}$ that correspond to the $N_l<N$ cells belonging to $D_l$. More precisely, the *MT-BCS* solution at the $f_{l+1}$ *FH* stage is aimed at retrieving the reduced vector of hyper-parameters

$$\hat{\mathbf{a}}_{l+1}=\left\{\hat{a}_{l+1,n}; n=1,...,N_l\right\}\ \text{subject to}\ \mathbf{r}_n\in D_l\,. \tag{7}$$

The *FH-MT-BCS* is terminated once one of the following conditions is met: (*i*) the last frequency step has been processed (i.e., $l=L$) or (*ii*) $\left|A_l-A_{l-1}\right|/\left|A_l\right|\le\eta$, where $A_l$ and $A_{l-1}$ denote the area of $D_l$ and $D_{l-1}$, respectively, and $\eta$ is a suitable threshold.

## 3. Numerical results

The aim of this section is to assess the performances of the proposed *FH-MT-BCS* algorithm. Towards this end, a set of numerical experiments is reported by generating time-domain synthetic data through the *GprMax2D* simulator [5]. In order to quantify the quality of each reconstruction, the following integral error is computed at a reference frequency $\bar{f}$ arbitrarily chosen within the $\left[f_{\min}, f_{\max}\right]$ range

$$\chi_{tot}=\frac{1}{N}\sum_{n=1}^{N}\frac{\left|\tau\left(\mathbf{r},\bar{f}\right)-\hat{\tau}\left(\mathbf{r},\bar{f}\right)\right|}{\left|\tau\left(\mathbf{r},\bar{f}\right)+1\right|}\,. \tag{8}$$

The investigation domain $D_{inv}$ is a square of 0.8 m centred at (0,-0.4) m. $V=20$ *z*-oriented infinitely long line sources at fixed height above the interface are used to illuminate it, while $M=19$ probes co-located with the sources are considered at each view to collect the scattered data. Moreover, $D_{inv}$ is filled with a lossy medium with relative permittivity $\varepsilon_{rb}=4.0$ and conductivity $\sigma_b=0.001$ S/m. $L=9$ uniformly spaced frequency samples are extracted from the computed *GPR* spectrum within the $\left[f_{\min}, f_{\max}\right]=\left[200, 600\right]$ MHz bandwidth, while $\bar{f}=400$ MHz.

### *3.1. Performances against noise*

The first set of experiments deals with the retrieval of a buried scatterer composed by two diagonal pixels with relative permittivity $\varepsilon_r^{obj}=5.0$ and conductivity of $\sigma_b=0.001$ S/m [Fig. 1(*a*)]. Figure 1 shows the retrieved dielectric profiles by the *FH-MT-BCS* when considering an additive white Gaussian noise on the measured time-domain total field with a signal-to-noise ratio defined as in [6] and equal to $SNR=60$ dB [Fig. 1(*b*)] and $SNR=40$ dB [Fig. 1(*d*)].

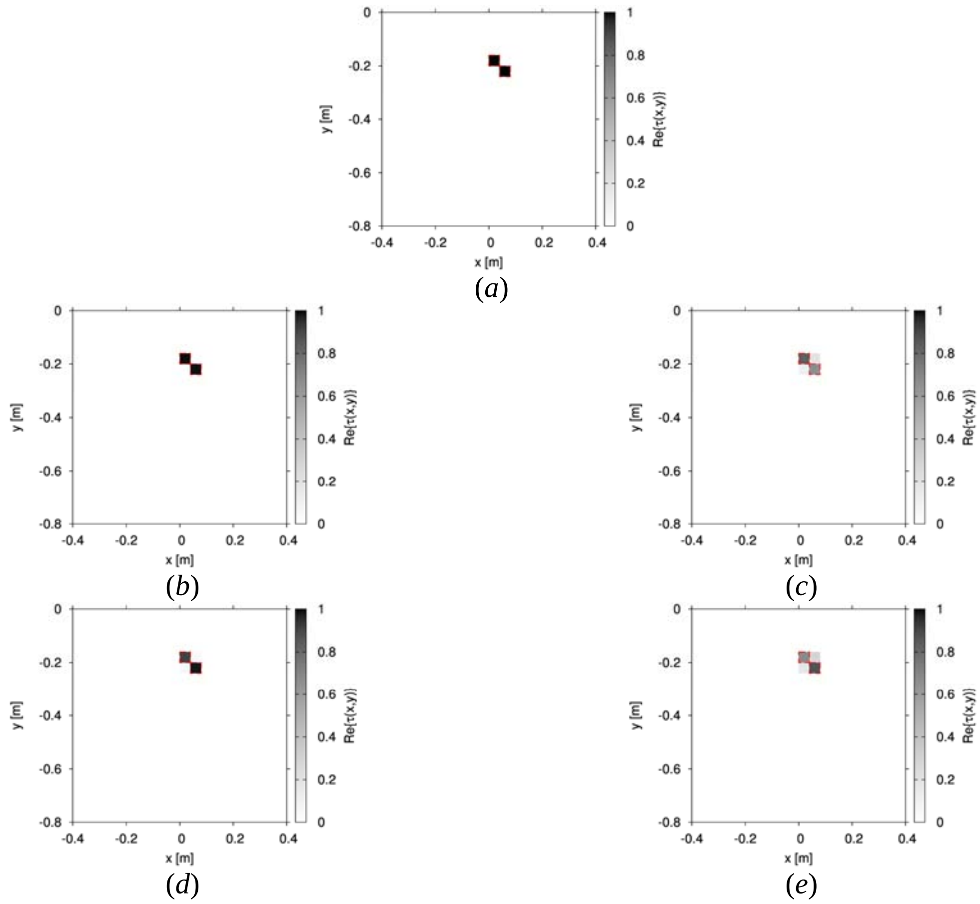


**Figure 1.** *Numerical Assessment* (*Two diagonal pixels scatterer,* $\varepsilon_r^{obj} = 5.0$, $\sigma^{obj} = 0.001$ S/m) – (*a*) Actual dielectric profile and retrieved solution by (*b*)(*d*) the *FH-MT-BCS* and (*c*)(*e*) the *FH-ST-BCS* methods for (*b*)(*c*) $SNR = 60$ dB and (*d*)(*e*) $SNR = 40$ dB on time-domain total field.

The reconstructions obtained by a single-task *BCS* implementation (*FH-ST-BCS*) are reported, as well [$SNR = 60$ dB - Fig. 1(*c*); $SNR = 40$ dB - Fig. 1(*e*)], this latter not imposing any correlation among the several views in solving (6). As it can be seen, the *FH-MT-BCS* significantly overcomes the *FH-ST-BCS*, as it is also visible by looking at the computed errors vs. the $SNR$ reported in Fig. 2.

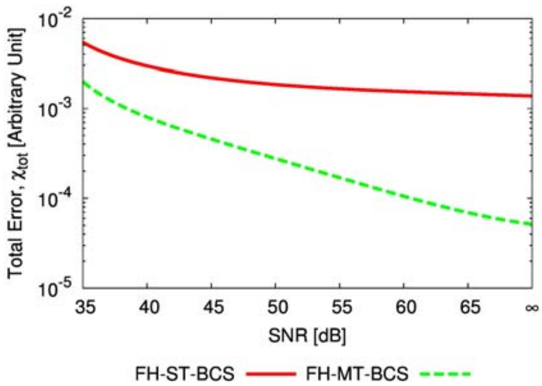


**Figure 2.** *Numerical Assessment* (*Two diagonal pixels scatterer,* $\varepsilon_r^{obj} = 5.0$, $\sigma^{obj} = 0.001$ S/m) – Behaviour of the reconstruction error versus the *SNR* on time-domain total field.

### *3.2. Performances against the relative permittivity of the buried targets*

This second set of numerical benchmarks is aimed at assessing the performances of the *FH-MT-BCS* when considering a variation of the relative permittivity of the unknown buried objects in $D_{inv}$ .

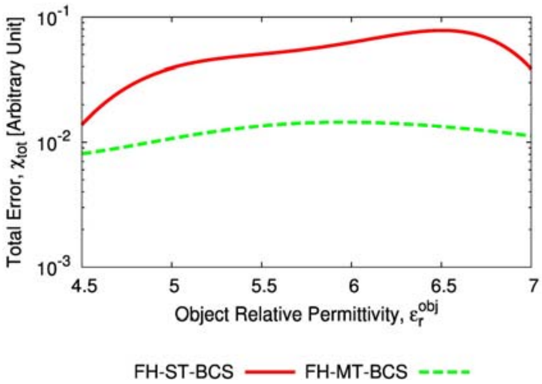


**Figure 3.** *Numerical Assessment* (*Two bars scatterer,* $\sigma^{obj} = 0.001$ S/m, $SNR = 35$ dB) – Behaviour of the reconstruction error versus the relative permittivity of the object.

Towards this end, Figure 3 compares the reconstruction errors made by the *FH-MT-BCS* and the *FH-ST-BCS* methods when dealing with the reconstruction of two separated sparse targets whose relative permittivity is varied in the range $\varepsilon_r^{obj} \in [4.5, 7.0]$ [$\sigma^{obj} = 0.001$ S/m - Fig. 4(*a*)] and considering noisy data with $SNR = 35$ dB.

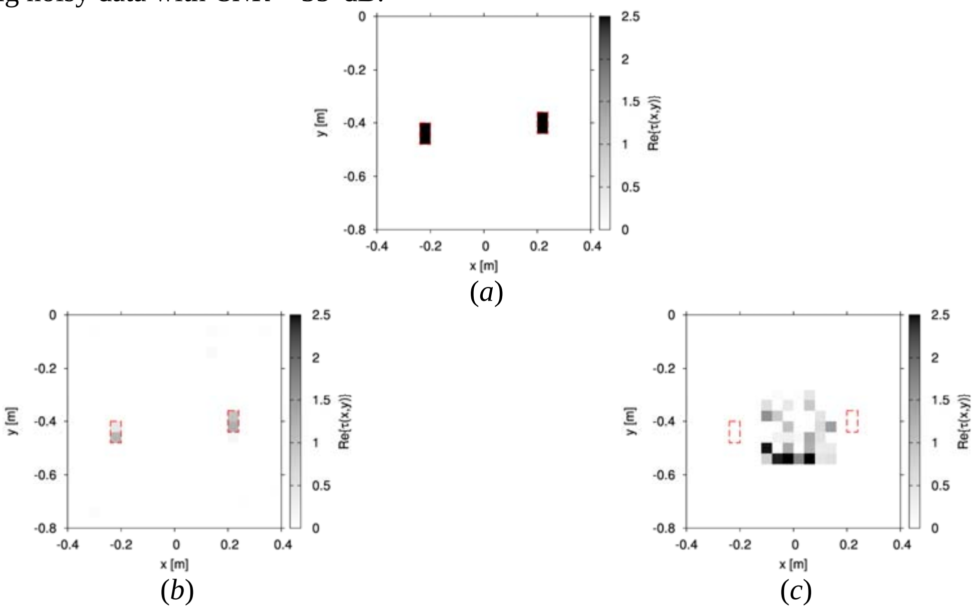


**Figure 4.** *Numerical Assessment* (*Two bars scatterer,* $\varepsilon_r^{obj} = 6.5$, $\sigma^{obj} = 0.001$ S/m, $SNR = 35$ dB) – (*a*) actual dielectric profile and retrieved solutions by the (*b*) *FH-MT-BCS* and (*c*) *FH-ST-BCS* techniques.

As it can be observed, lower errors are obtained by the *FH-MT-BCS* in all cases (Fig. 3). As a matter of fact, significantly better reconstructions are provided by the proposed method despite the non-negligible amount of noise, as it can be seen by looking at the retrieved profiles in Fig. 4 for $\varepsilon_r^{obj} = 6.5$. Even if providing a slight underestimation of the contrast, the *FH-MT-BCS* is able to correctly detect the scatterer support [Fig. 4(*b*)], while the single-task version yields an unsatisfactory result [Fig. 4(*c*)].

## 4. Conclusions

An innovative inverse scattering technique has been presented in order to deal with the retrieval of the dielectric characteristics of a buried investigation domain starting from wide-band *GPR* measurements. The proposed *FH-MT-BCS* methodology efficiently combines the information coming from multi-chromatic data thanks to an innovative initialization strategy of the *RVM* solver, as well as benefits from the regularization capabilities of the *MT-BCS* solver. The main novelty of the work is the innovative integration of the *MT-BCS* within the *FH* strategy in order to progressively exploit the acquired information about the solution at the low-pass reconstructions, thanks to the introduction of a customized "constrained" *RVM* solver. Some numerical results have been presented, in order to validate the effectiveness of the *FH-MT-BCS*, as well as to show its superior performances with respect to a single task-based solution within the same framework. Future work will be devoted at extending the developed algorithm to deal with more realistic scenarios by considering, for example, a non-static behaviour of both object and soil electromagnetic properties, the presence of metallic/PEC scatterers, as well as a full three-dimensional formulation of the subsurface scattering equations.

## References

[1] Lesselier D and Habashy T 2000 Special issue on electromagnetic imaging and inversion on the Earth's subsurface *Inverse Probl.* **16**
[2] Chew W C and Lesselier D 2004 Special issue on electromagnetic characterization of buried obstacles *Inverse Probl.* **20**
[3] Chen C-C, Johnson J T, Sato M and Yarovoy A G 2007 Special issue on subsurface sensing using ground-penetrating radar *IEEE Trans. Geosci. Remote Sens.* **45** 2419–2421
[4] Peters L, Daniels J and Young J D 1994 Ground penetrating radar as a subsurface environmental sensing tool *IEEE Proc.* **82** 1802–1822
[5] Soldovieri F, Solimene R, Lo Monte L and Bavusi M 2011 Sparse reconstruction from GPR data with applications to rebar detection *IEEE Trans. Instr. Meas.* **60** 1070-1079
[6] Salucci M, Oliveri G and Massa A 2015 GPR prospecting through an inverse scattering frequency-hopping multifocusing approach *IEEE Trans. Geosci. Remote. Sens*. **53** 6573-6592
[7] Salucci M, Poli L and Massa A 2017 Advanced multi-frequency GPR data processing for non-linear deterministic imaging *Signal Processing* **132** 306-318
[8] Persico R and Sodovieri F 2008 Effects of background removal in linear inverse scattering *IEEE Trans. Geosci. Remote Sens.* **46** 1104-1114
[9] Rocca P, Benedetti M, Donelli M, Franceschini D and Massa A 2009 Evolutionary optimization as applied to inverse scattering problems *Inverse Probl.* **25** 1-41
[10] Salucci M, Poli L, Anselmi N and Massa A 2017 Multifrequency particle swarm optimization for enhanced multiresolution GPR microwave imaging *IEEE Trans. Geosci. Remote Sens.*, in press
[11] Massa A, Rocca P and Oliveri G Compressive sensing in electromagnetics - A review *IEEE Antennas Propag. Mag.* **57** 224-238
[12] Anselmi N, Oliveri G, Hannan M A, Salucci M and Massa A 2017 Color compressive sensing imaging of arbitrary-shaped scatterers *IEEE Trans. Microw. Theory Techn.*, in press
[13] Anselmi N, Oliveri G, Salucci M and Massa A 2015 Wavelet-based compressive imaging of sparse targets *IEEE Trans. Antennas Propag.* **63** 4889-4900

## Acknowledgment

This work has been partially supported by the SIRENA project (2014-2017) funded by DIGITEO (France) under the "Call for Chairs 2014" and benefited from the networking activities carried out within the EU funded COST Action TU1208 "Civil Engineering Applications of Ground Penetrating Radar".